JOURNAL OF APPLIED ELECTROCHEMISTRY **28** (1998) 511–516

Simultaneous determination of chlorine and oxygen evolving at RuO_2/Ti and RuO_2–TiO_2/Ti anodes by differential electrochemical mass spectroscopy

T. ARIKAWA, Y. MURAKAMI, Y. TAKASU

Department of Fine Materials Engineering, Faculty of Textile Science and Technology, Shinshu University, 3-15-1 Tokida, Ueda 386, Japan

Received 18 November 1996; revised 27 March 1997

Chlorine and oxygen evolving at RuO_2/Ti and RuO_2–TiO_2/Ti anodes have been simultaneously determined at electrode potentials from 1.0 to about 2 V (vs Ag/AgCl) by differential electrochemical mass spectroscopy (DEMS). On the RuO_2/Ti anodes, the threshold electrode potential for oxygen evolution increased with a decrease in RuO_2 loading, while the chlorine evolution potential was unchanged. Low RuO_2 loading anodes gave a high chlorine evolution ratio under various constant electrolysis potentials. On the RuO_2–TiO_2/Ti anodes, the threshold electrode potential for oxygen evolution increased with an increase in the TiO_2 content more remarkably than that for chlorine evolution. High TiO_2 content anodes gave a high chlorine evolution ratio at various constant electrolysis potentials. The combination of RuO_2 and TiO_2 exhibits a remarkable effect with respect to the enhancement of chlorine evolution selectivity.

Keywords: *ruthenium oxide*, *titanium oxide*, *chlorine*, *oxygen*, *DEMS*, *porous electrode*

1. Introduction

RuO_2-based oxide coated titanium electrodes are important anodes in the chlor-alkali industry [1]. TiO_2 and IrO_2 are predominantly used as additives to increase the activity, selectivity and stability of the electrodes toward chlorine evolution [2–6].

Because RuO_2 is an active electrocatalyst for oxygen evolution, as well as for chlorine evolution [7], the two parallel electrochemical reactions can occur at the RuO_2-based oxide anodes. The standard electrode potentials of the reactions [8] are

$$Cl_2 + 2e^- \rightleftharpoons 2Cl^- \qquad E_0 = 1.358\,V(25\,^\circ C)$$

and

$$O_2 + 4H^+ + 4e^- \rightleftharpoons 2H_2O \qquad E_0 = 1.229\,V(25\,^\circ C)$$

The rate of these reactions depends on the concentration of the chloride ion in the electrolyte and on the oxide composition of the anodes. In an early work on the chlorine-to-oxygen evolution ratio at anodes, the ratio was shown to be depressed in the low-current density region [2]. However, the effect of the anode oxide composition on the chlorine evolution selectivity has not yet been fully clarified. Thus, the simultaneous determination of chlorine and oxygen in the competitive evolution will assist in understanding the effect.

Differential electrochemical mass spectroscopy (DEMS) [9–12] developed by Wolter and Heitbaum is advantageous for online identification and quantitative detection of the electrochemical products and intermediates. Wohlfahrt–Mehrens and Heitbaum applied the DEMS technique to an oxygen isotope study of oxygen evolution at RuO_2 anodes [10]. The present authors have previously applied this technique to a RuO_2–TiO_2/Ti anode and determined both the threshold electrode potentials of the individual evolutions (chlorine and oxygen) and the chlorine evolution ratio, $R(Cl_2)$, in NaCl solution.

In this paper, competitively evolving chlorine and oxygen were simultaneously determined by the DEMS technique for the RuO_2–TiO_2/Ti anode system under relatively low NaCl concentration conditions. The present paper discusses the dependencies of oxide loading, anode oxide composition and chloride ion concentration on both the threshold electrode potentials for each gas evolution and the chlorine evolution ratio.

2. Experimental details

2.1. *Samples*

Substrates of the oxide-coated electrodes were 99.5% titanium rods 1.6 mm (diam.) × 150 mm in size. They were etched in 10% aqueous oxalic acid at 80 °C for 1 h, washed ultrasonically with distilled water and then dried. The oxide electrodes were prepared by repetition of the following coating process ten times: dipping of the substrate into the *n*-butanol solution of the mixture of 0.53 M $RuCl_3$ and 1.04 M $Ti(OBu)_4$, drying at 60 °C for 10 min, and thermal decomposition of the coated metal salts and butoxide at 450 °C for 10 min.

The oxide loading was determined by weight difference before and after electrode preparation [13]. The measured oxide loadings of the RuO_2/Ti electrodes were prepared with different solutions of $RuCl_3$–*n*-BuOH solution concentrations (0.067–1.06 M), about 0.1–0.9 mg cm^{-2}, and those of the RuO_2–TiO_2/Ti electrodes prepared with different compositions of $RuCl_3$–Ti-$(OBu)_4$–*n*-BuOH solutions were about 0.5–0.7 mg cm^{-2}.

To adjust the apparent surface area of the electrode to 0.5 cm^2, the excess area of the oxide film was removed prior to the electrochemical measurements.

2.2. *DEMS system and measurements*

The DEMS system used in this study is shown in Fig. 1. The electrochemical cell was separated from the vacuum line by a porous PTFE membrane (100 μm in thickness, Japan Gore-Tex Co., Ltd) supported by a glass tube with a pin hole. An oxide electrode was placed against the PTFE membrane. The counter electrode and reference electrode in the electrochemical cell were a platinum net and a Ag/AgCl electrode, respectively. The electrolyte was an aqueous solution of NaCl + 0.1 M $HClO_4$, which was carefully purged of air with Ar gas and kept at 25 °C. To maintain the concentration and temperature as constant as possible, the electrolyte solution was slowly circulated between a reservoir and a cell (~20 ml min^{-1}), where 300 ml of electrolyte solution was used. The amount of chloride ion in the electrolyte gradually decreased in duration of the electrolysis; however, the total amount of chloride ion oxidized to chlorine gas after the electrolysis corresponded to 4%, at the greatest, of the initial amount of chloride ion in the electrolyte ([NaCl] = 0.3 M + [$HClO_4$] = 0.1 M). The gaseous products generated at the oxide electrodes were sucked into the vacuum line through the hydrophobic porous PTFE membrane and introduced to the quadrupole mass spectrometer (MSQ-101, ULVAC Corp.). During the measurements, the amounts of each product were followed by mass intensity, i_m, and current density, i. The sweep rate of the electrode potential was 0.1 mV s^{-1}, sufficiently slow to follow the change in the amount of the products against the low diffusion speed through the PTFE membrane. The lag time was within about 30 s.

A potentiostat (HA-151, Hokuto Denko) and a function generator (HB-104, Hokuto Denko) were used for the voltammetric measurements. *IR* compensation was carried out by the current-interruption technique after a series of DEMS measurements with solution resistance using a Solartron 1286 electrochemical interface (Solartron Corp.).

2.3. *Evaluation of the threshold potentials for the gas evolutions*

Figure 2 shows a typical voltammetric curve, E/i, and the mass detection curves, E/i_m, for Cl^+ ($m/e = 35$) and O_2^+ ($m/e = 32$) for the RuO_2(100%)/Ti electrode. The threshold electrode potentials for the evolution of each product were evaluated from the curves, where

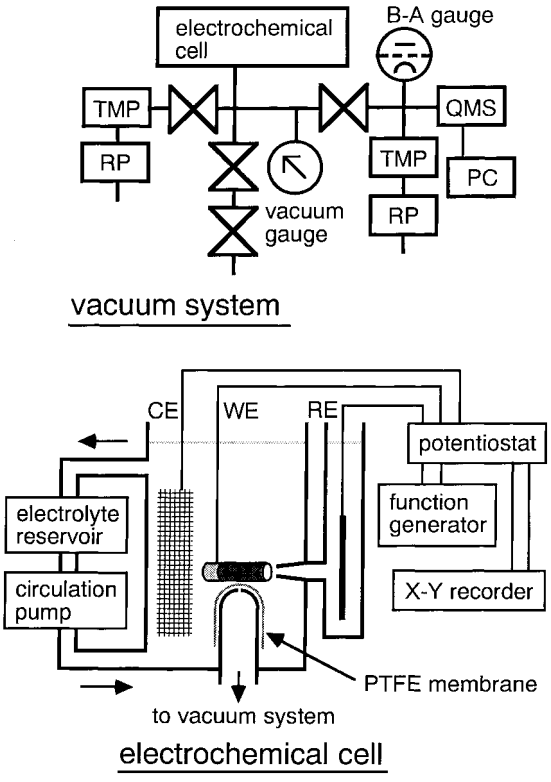

Fig. 1. The DEMS system: (a) Pumping system: QMS, quadrupole mass spectrometer; RP, rotary pump; TMP, turbo molecular pump; PC, personal computer. (b) Electrochemical cell: WE, working electrode; CE, counter electrode; RE, reference electrode.

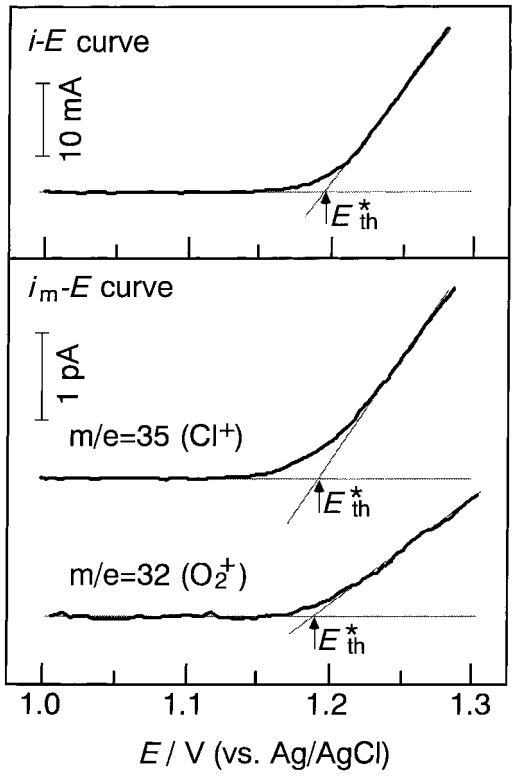

Fig. 2. The voltammetric current, i, and the mass detective current i_m, for Cl^+ ($m/e = 35$) and O_2^+ ($m/e = 32$) against electrode potential, E. Working electrode was RuO_2(100%)/Ti. Electrolyte was an aqueous solution of 0.3 M NaCl + 0.1 M $HClO_4$. Potential sweep 0.1 mV s^{-1}.

the threshold potential, E^*_{th}, was the intercept of the extrapolation of the linear part of the E/i_m curve.

2.4. *Evaluation of the chlorine evolution ratio $R(Cl_2)$*

The chlorine evolution ratio, $R(Cl_2)$, was calculated from the ratio of the amount of chlorine mass intensity to that of the mass intensity of total products, after about 8 min holding at each constant electrode potential. Although the detected gas at QMS was a part of all the products, the gas translation ratios of chlorine and oxygen for the PTFE membrane were previously measured at QMS, and the chlorine evolution ratio, $R(Cl_2)$, can be determined using the previously determined value. The standard deviation of data was about 0.1. The $i_{O_2}, i_{Cl_2}/E$ curves for some anodes were estimated based on both the i/E curves and each gas evolution ratio determined by DEMS.

3. Results and discussion

3.1. *Chloride ion concentration effect*

Figure 3 shows the threshold potentials of both chlorine and oxygen evolutions evaluated on a RuO_2/Ti anode (the oxide loading is about 0.5 mg cm^{-2}) in various NaCl concentrations. Threshold potentials for chlorine evolution decreased with an increase in chloride concentration, while those for oxygen evolution increased. The i/E and $i_{O_2}, i_{Cl_2}/E$ curves on the RuO_2/Ti anode in a dilute NaCl solution and those in a concentrated solution are shown in Fig. 4(a) and (b), respectively. These show that both the selectivity of the chlorine evolution and the current density depend on the Cl^- concentration. Figure 5 shows the chlorine evolution ratio, $R(Cl_2)$, against the electrode potential on the RuO_2/Ti anode in solutions with various Cl^- concentrations. In order to clarify the character of this oxide electrode system for chlorine evolution selectivity, an electrolyte of fairly low concentration of NaCl (0.3 M) was used, although this condition is considerably different from that in industrial electrolysis.

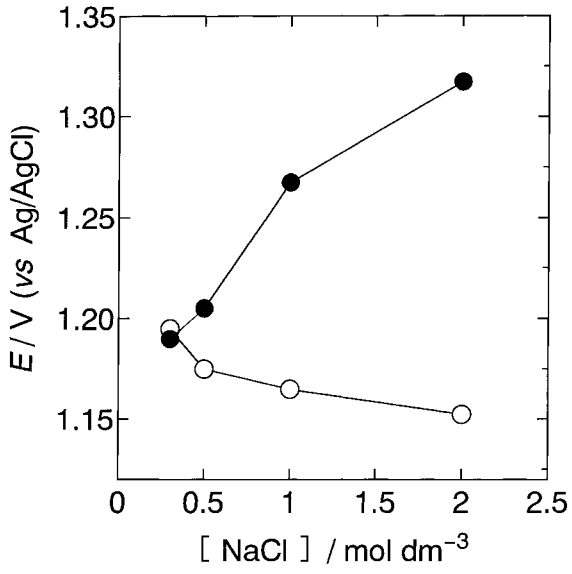

Fig. 3. Threshold potential for each gas evolution against Cl^- concentration of NaCl aqueous solution with the 0.1 M $HClO_4$ on RuO_2(100%)/Ti electrode. Potential sweep 0.1 mV s^{-1}. Key: (○) threshold potential $E^*_{th}(Cl_2)$ for chlorine evolution; (●) threshold potential $E^*_{th}(O_2)$ for oxygen evolution.

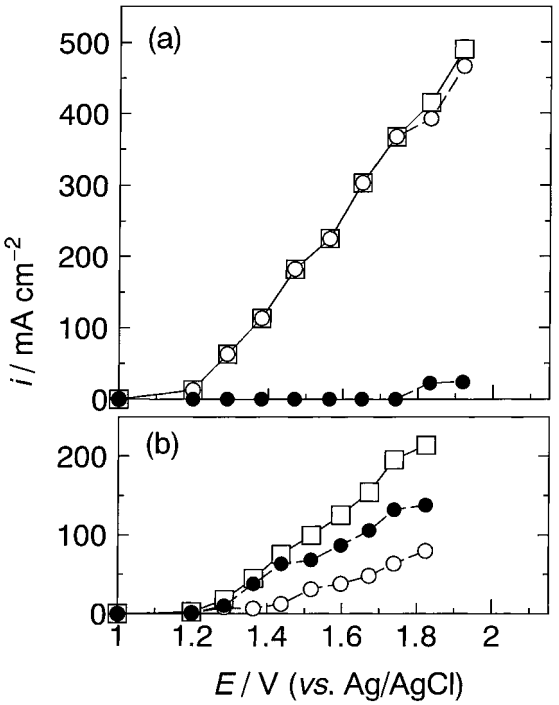

Fig. 4. i/E (□) and i_{Cl_2}/E (○), i_{O_2}/E (●) curves for RuO_2/Ti electrodes in different concentrations of Cl^-: (a) [Cl^-] 2 M, (b) [Cl^-] 0.3 M for RuO_2/Ti electrode.

3.2. *Oxide loadings of RuO_2/Ti electrode*

As shown in Fig. 6, the threshold potentials, E^*_{th}, for the oxygen evolution considerably increased with a

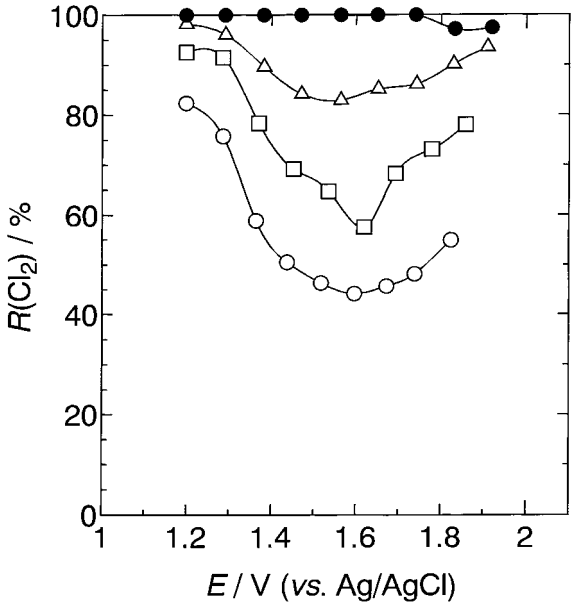

Fig. 5. Chlorine evolution ratio, $R(Cl_2)$, against electrode potential, E, for each of the Cl^- concentrations of NaCl aqueous solution with the 0.1 M $HClO_4$ for RuO_2/Ti electrode. Key: (○) 0.3, (□) 0.5, (△) 1 and (●) 2 M NaCl.

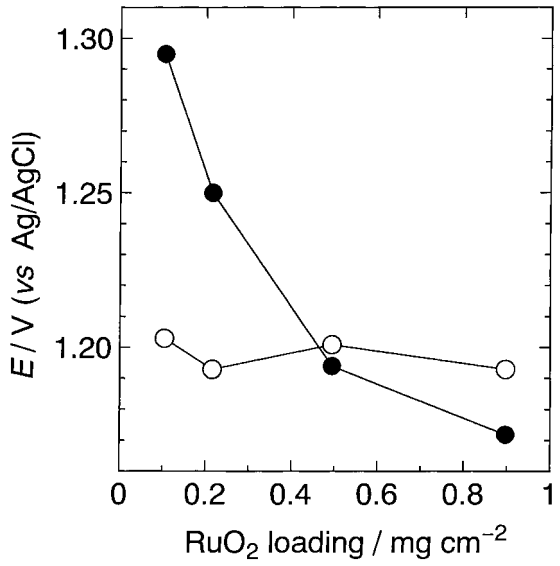

Fig. 6. Threshold potentials (a) $E^*_{th}(Cl_2)$ for chlorine evolution, and (b) $E^*_{th}(O_2)$ for oxygen evolution against the RuO_2 loading of RuO_2/Ti anode. Potential sweep 0.1 mV s^{-1}.

decrease in the RuO_2 loadings on RuO_2/Ti anode, while the threshold potentials, E^*_{th}, for the chlorine evolution remained unchanged.

Figure 7 shows the i/E and $i_{O_2}, i_{Cl_2}/E$ curves for two oxide loading RuO_2/Ti anodes: (a) RuO_2 (0.1 mg cm^{-2})/Ti and (b) RuO_2 (0.9 mg cm^{-2})/Ti. Figure 8 shows the chlorine evolution ratio, $R(Cl_2)$, against the electrode potential for these oxide-coated electrodes. Though the total current density was not proportional to the oxide loading, it increased with an increase in the RuO_2 loading. The electrolysis proceeded not only on the outer part of the porous RuO_2 layer, but also on its inner part, while the

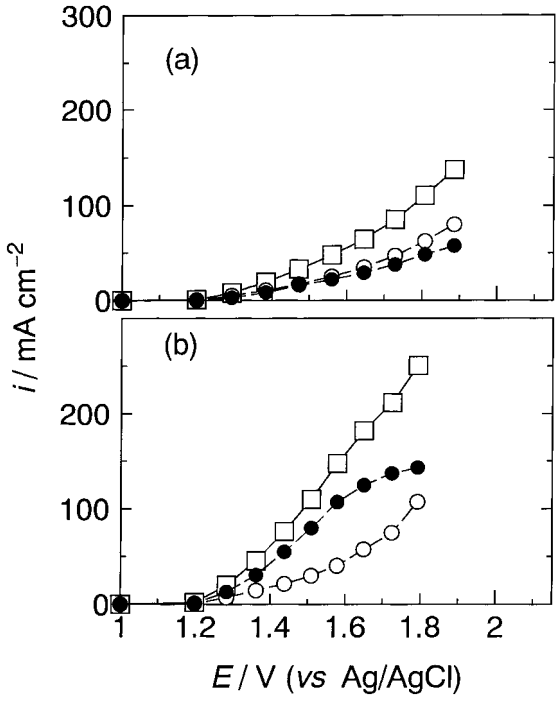

Fig. 7. i/E (□) and i_{Cl_2}/E (○), i_{O_2}/E (●) curves for two RuO_2/Ti electrodes with different amount of oxide loading: (a) 0.1 and (b) 0.9 mg cm^{-2} RuO_2/Ti.

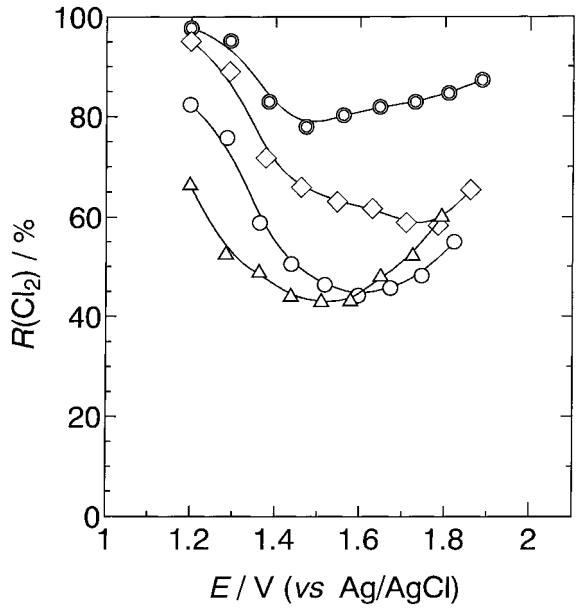

Fig. 8. Chlorine evolution ratio, $R(Cl_2)$, against electrode potential, E, for each loading of RuO_2/Ti anode. Key: (◎) 0.1, (◇) 0.2, (○) 0.5 and (△) 0.9 mg cm^{-2} RuO_2.

contribution of the inside part of the oxide layer to the total chlorine evolution would be relatively low (Fig. 7). The comparison of Fig. 7(a) with Fig. 7(b) suggests that the increase in RuO_2 loading resulted in the increase in the oxygen evolution ratio.

In spite of the same composition (RuO_2/Ti), the chlorine evolution selectivities of these oxide electrodes depended on the amount of oxide loading. This may be attributed to the porous structure of the oxide electrodes as will be described below.

The oxide loading of the RuO_2/Ti anode was controlled by the concentration of the $RuCl_3$ solution used for the sample preparation. Because the surface electric charge of the anode was almost proportional to the RuO_2 loading, as shown in Fig. 9, the concentration of the $RuCl_3$ solution seems to scarcely affect the size of the RuO_2 particles and the microstructure of the RuO_2 layer. The variation of the oxide loading probably affected only the ratio of the inner to the outer surface.

Burke and Murphy [14] and Trasatti *et al.* discussed the mass transfer effect about the inner and outer surfaces of the porous RuO_2 electrodes [15]. The former group found that the chlorine gas evolution reaction is independent of the oxide loading of the RuO_2/Ti anode, and apparently depends on the external surface area. On the contrary, the oxygen evolution current density was proportional to the oxide loading of the electrode. They explained that the main factor influencing the rate of chlorine evolution was assumed to be the transfer of chlorine gas away from the electrode surface. This interpretation may be valid for the evolution behaviour of oxygen and chlorine in this investigation. Additionally, if some chlorine evolved even at the inner part of the oxide layer, it is possible that the diffusing chloride ions from the external surface are significantly

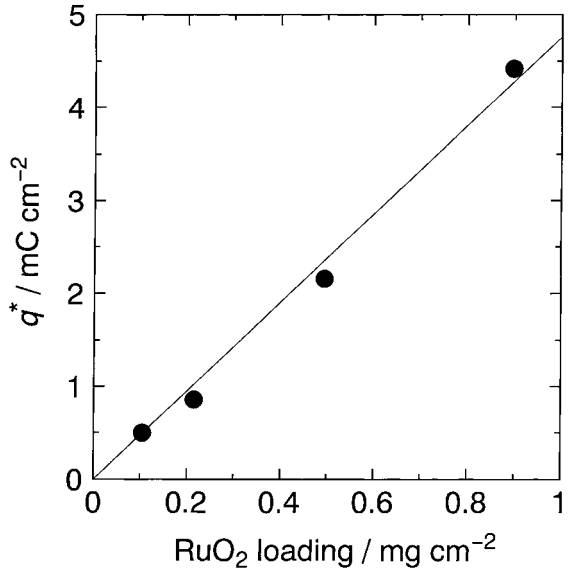

Fig. 9. Surface electric charge of anode against RuO_2 loading in 0.5 M H_2SO_4. Potential sweep range and potential sweep rate 0.3–1.1 V vs RHE and 50 mV s^{-1}, respectively.

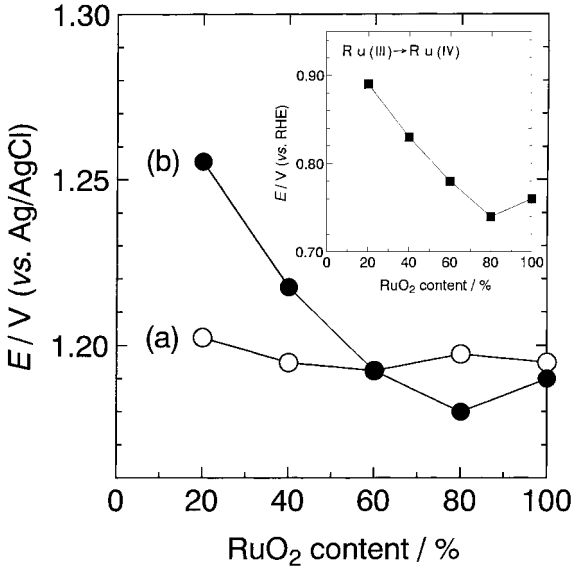

Fig. 11. Threshold potentials (a) $E^*_{th}(Cl_2)$ for chlorine evolution and (b) $E^*_{th}(O_2)$ for oxygen evolution against the RuO_2 content of RuO_2–TiO_2/Ti anode. Potential sweep 0.1 mV s^{-1}. The inset expresses an oxidation peak potential of (Ru(III) ⇌ Ru(IV) on the RuO_2–TiO_2/Ti anodes in 0.5 M H_2SO_4.

consumed to form Cl_2 before they arrive at the inner part (Fig. 10). However, this explanation does not account for the origin of the threshold potential changes in oxygen evolution.

3.3. *RuO_2–TiO_2/Ti electrode*

As shown in Fig. 11, the threshold potential, E^*_{th}, for oxygen evolution considerably increased with an increase in the TiO_2 content, while those for chlorine evolution remained unaltered or slightly increased. Although the same measurements were performed for the TiO_2/Ti electrode, evolution of neither oxygen nor chlorine was observed. The inset of Fig. 11 expresses an oxidation peak potential of Ru(III) ⇌ Ru(IV) on the RuO_2–TiO_2/Ti anodes in 0.5 M H_2SO_4. The dependence of the peak potentials on the RuO_2 content is similar to that of the oxygen evolution potentials. Because the oxygen evolution on the ruthenium oxide relates to the oxidation of metal ion in a crystal lattice [16], the oxidation states of Ru in the lattice should affect the oxygen evolution behaviour. That is, the oxygen evolution potential is governed by the redox property of the oxide and reflects on the selectivity of the oxide electrode for chlorine evolution.

Figure 12 shows the i/E and i_{O_2}, I_{Cl_2}/E curves for two typical RuO_2–TiO_2/Ti anodes: (a) RuO_2(20%)–TiO_2(80%)/Ti and (b) RuO_2(80%)–TiO_2(20%)/Ti. In spite of the small content of RuO_2, the current density for oxygen evolution on the TiO_2-rich anode was

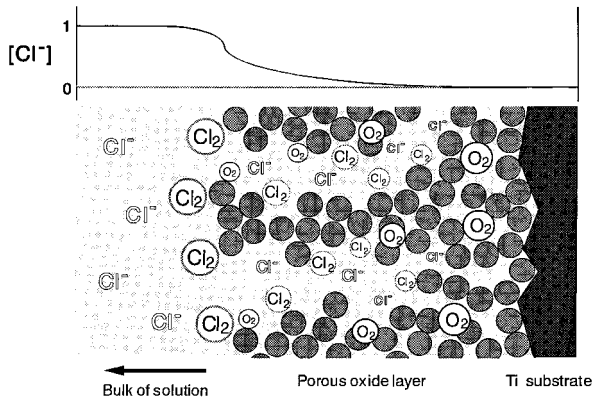

Fig. 10. A model of competitive evolution of chlorine and oxygen on and in the porous oxide layer of RuO_2/Ti anode. The grey circle represents the RuO_2 particle. The size of the outline letters Cl^- on a light grey background express the Cl^- concentration. The size of the letters Cl_2 and O_2 represent the degree of chlorine and oxygen evolution, respectively.

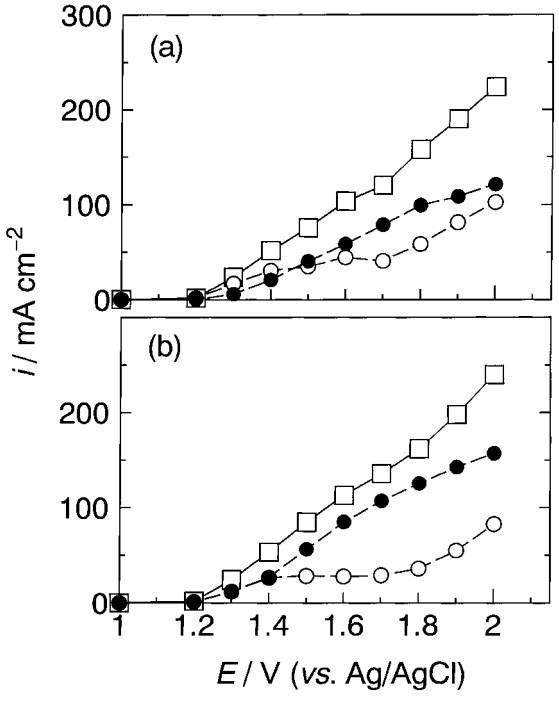

Fig. 12. The i/E (□), i_{Cl_2}/E (○) and i_{O_2}/E (●) curves for two RuO_2–TiO_2/Ti electrodes with different oxide composition. (a) RuO_2(20%)–TiO_2(80%)/Ti, (b) RuO_2(80%)–TiO_2(20%)/Ti.

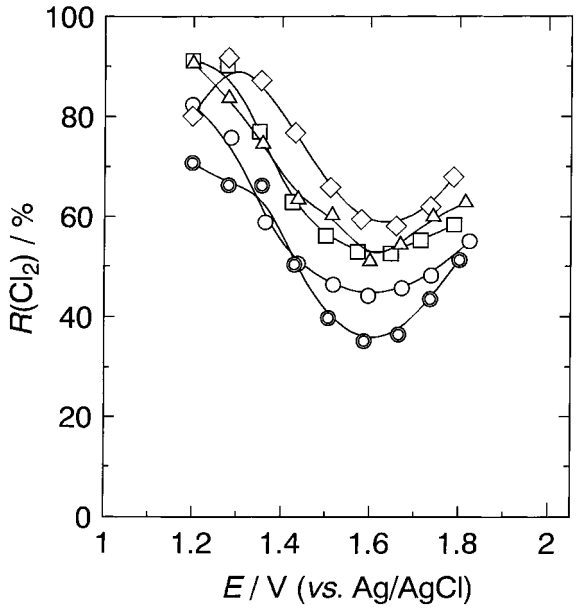

Fig. 13. Chlorine evolution ratio, $R(Cl_2)$, against electrode potential, E, for each RuO_2 content of RuO_2–TiO_2/Ti anode. Key: (○) 100%, (◎) 80%, (□) 60%, (◇) 40% and (△) 20% RuO_2.

almost equivalent to that of the RuO_2-rich anode. This may be due to the existence of mud cracks on the anode surface. Mud cracks of the order of micrometers were not observed on the RuO_2-rich electrode, while many mud cracks were seen on the TiO_2-rich electrode [17]. Mud cracks contribute to an extension of the outer surface of the electrode. It is noted that the chlorine evolution current on the TiO_2-rich anode was larger than that of the RuO_2-rich anode.

The chlorine evolution ratios, $R(Cl_2)$, against the electrode potential are shown in Fig. 13 as a function of the compositions of RuO_2 for the RuO_2–TiO_2/Ti anodes. The RuO_2(40%)–TiO_2(60%)/Ti anode gives the greatest chlorine evolution ratio, $R(Cl_2)$, and the largest current density. Generally, the chlorine evolution ratio, $R(Cl_2)$, for these electrodes increases with an increase in the TiO_2 content; however, the anodes with a small TiO_2 content give a lower chlorine evolution ratio and lower voltammetric current density. It is evident that the combination of RuO_2 and TiO_2 leads to the advantage of the chlorine evolution over the oxygen evolution.

4. Conclusions

The competitive evolution of chlorine and oxygen at various compositions of RuO_2–TiO_2/Ti anodes was simultaneously determined by a DEMS technique, and their threshold electrode potentials for each gas and the chlorine evolution ratio, $R(Cl_2)$, were evaluated.

The comparison of the voltammetric current, i, with the chlorine evolution ratio, $R(Cl_2)$, for the RuO_2–TiO_2/Ti anodes suggests that the combination of RuO_2 and TiO_2 led to the advantage of the chlorine evolution over the oxygen evolution.

The selectivity of chlorine evolution is influenced by the redox property of the oxide of RuO_2 and TiO_2, and it depends on the amount of loading of RuO_2 for the RuO_2/Ti electrodes. This must originate from both the mass transfer effect [18] and the other parameters [19], because the chlorine evolution was carried out mainly in a current range where mass transfer is the rate-determining step. The performance of DSA®-type electrodes must be affected by the mixed effects of the redox property of the oxide and the mass transfer effect. The change in the surface geometry, as well as the redox property, depends on the composition of their oxide layer; therefore, it is difficult to distinguish the 'oxide composition effect' from the 'mass transfer effect'.

Acknowledgements

The authors are grateful to Permelec Electrode Ltd, Japan, for providing the chemical reagents. They also wish to thank Japan Gore-Tex Ltd for a generous gift of the PTFE membrane. The present work was supported by a grant-in-aid for Scientific Research on Priority Areas 'Catalysis Chemistry of Unique Reaction Fields, Extreme Environment Catalysis' no. 07242239 from the Ministry of Education, Science and Culture, Japan.

References

[1] S. Trasatti, *Electrochim. Acta* **36** (1991) 225.
[2] F. Hine, M. Yasuda, T. Noda and T. Yoshida, *J. Electrochem. Soc.* **126** (1979) 1439.
[3] R. S. Yeo, J. Orehotsky, W. Visscher and Srinivasan, *ibid.* **128** (1981) 1900.
[4] A. de Battisti, G. Lodi, M. Cappadonia, G. Battaglin and R. Kotz, *ibid.* **136** (1985) 2596.
[5] M. Guglielmi, P. Colombo, V. Rigato, G. Battaglin, A. Boscolo-Boscoletto and A. de Battisti, *ibid.* **139** (1992) 1655.
[6] K. Kameyama, K. Tsukada, K. Yahikozawa and Y. Takasu, *ibid.* **141** (1993) 643.
[7] Ch. Comninellis and G. P. Vercesi, *J. Appl. Electrochem.* **21** (1994) 335.
[8] A. J. Bard (Ed), 'Encyclopedia of Electrochemistry of the Elements', Vol. 4 Mercel Dekker, New York (1973), p. 193.
[9] O. Wolter and J. Heitbaum, *Ber. Bunsenges. Phys. Chem.* **88** (1984) 2.
[10] M. Wohlfahrt-Mehrens and J. Heitbaum, *J. Electroanal. Chem.* **237** (1987) 251.
[11] H. Kita and Y. Gao, *Catalyst* (*Catalysis Society of Japan*; *in Japanese*) **36** (1994) 213.
[12] Y. Takasu, T. Arikawa, S. Sunohara and K. Yahikozawa, *J. Electroanal. Chem.* **361** (1993) 279.
[13] S.-M. Lin and T.-C. Wen, *Electrochim. Acta* **39** (1994) 393.
[14] L. D. Burke and O. J. Murphy, *J. Electroanal. Chem.* **96** (1979) 19.
[15] S. Ardizzone, G. Fregonara and S. Trasatti, *Electrochim. Acta* **35** (1990) 263.
[16] K. Doblhofer, M. Metikos, Z. Ogumi, and H. Gerischer, *Ber. Bunsenges. Phys. Chem.* **82** (1978) 1046.
[17] K. Tsukada, K. Kameyama, K. Yahikozawa and Y. Takasu, *Denki Kagaku* (*J. Electrochemical. Society of Japan, Japanese*) **61** (1993) 435.
[18] R. White and J. Newman, *J. Electroanal. Chem.* **82** (1977) 173.
[19] V. V. Losev, N. Y. Bune and L. E. Chuvaeva, *Electrochim. Acta* **34** (1988) 929.